ACS Catalysis

Research Article

pubs.acs.org/acscatalysis

Establishing a Link between Well-Ordered Pt(100) Surfaces and Real Systems: How Do Random Superficial Defects Influence the Electro-oxidation of Glycerol?

Pablo S. Fernández,[*,†] Janaina Fernandes Gomes,[†,▽] Camilo A. Angelucci,[‡] Polina Tereshchuk,[†] Cauê A. Martins,[§] Giuseppe A. Camara,[∥] María E. Martins,[⊥] Juarez L. F. Da Silva,[†] and Germano Tremiliosi-Filho[†]

[†]São Carlos Institute of Chemistry, University of São Paulo, P.O. Box 780, 13560-970 São Carlos, São Paulo, Brazil

[‡]Center of Natural and Human Sciences (CCNH), Federal University of ABC (UFABC), Av. dos Estados, 5001 Santo André, Brazil

[§]Faculty of Exact Sciences and Technology, Federal University of Grande Dourados, 79804-970 Dourados, Mato Grosso do Sul, Brazil

[∥]Institute of Chemistry, Federal University of Mato Grosso do Sul, C.P. 549, 79070-900 Campo Grande, Mato Grosso do Sul Brazil

[⊥]Physical Chemistry Research Institute (INIFTA), Exact Sciences Faculty, CCT La Plata-CONICET, C.P. 1900, La Plata, Argentina

Supporting Information

ABSTRACT: Glycerol (GlOH) accumulation and its very low price constitute a real problem for the biodiesel industry. To overcome these problems, it is imperative to find new GlOH applications. In this context, electrochemistry arises as an important alternative to the production of energy or fine chemicals using GlOH as a reactant. To make these opportunities a reality, it is fundamentally necessary to understand how the glycerol electro-oxidation reaction (GEOR) occurs on catalysts used in real systems. Thus, research using model surfaces has generated the first insight into the electrochemistry of extremely complex real catalysts. Accordingly, in this work, we generate Pt(100) disturbed surfaces in a reproducible manner, carefully controlling the surface defect density. Then, GEOR is studied on well-ordered Pt(100) and on the disturbed Pt(100) surfaces in 0.5 M H_2SO_4 using cyclic voltammetry (CV) and in situ Fourier transform infrared spectroscopy (FTIR). The CV profile of GEOR consists of a single peak in the positive scan. The onset reaction displays the influence of defects present on the surface. On a surface with a high degree of disorder, the main GlOH oxidation process begins at 0.8 V vs RHE, whereas for well-ordered Pt(100), it starts 0.1 V earlier. FTIR experiments show the presence of carbon monoxide and carbonyl absorption bands. The electrochemical and spectroelectrochemical results are supported by density functional theory calculations showing that both CO and GlOH bind more strongly on disturbed than on well-ordered surfaces. Thus, our experiments show that Pt−CO (or other GlOH residue) bond breaking may be the GEOR rate-determining step.

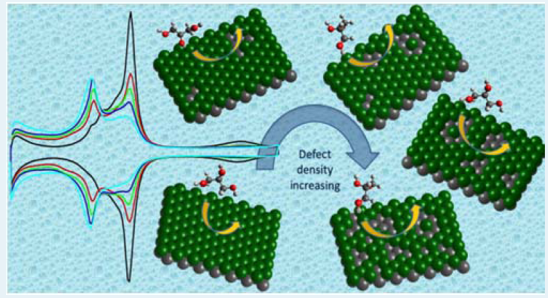

KEYWORDS: *glycerol electro-oxidation reaction, platinum single crystals, disordered surfaces, in situ FTIR, density functional theory*

INTRODUCTION

Biodiesel has become a real sustainable source of energy to mitigate our dependence on petro-diesel fuel. However, biodiesel manufacturing leads us to reconsider how environmentally friendly this fuel is, given the volume of GlOH resulting from its production: approximately 1 kg of GlOH per 10 kg of biodiesel.[1] Due partially to the increase in biodiesel production in the past decade, the GlOH supply in the market has outstripped the normal demand (pharmaceutical, cosmetics, and food industries), causing a drop in the price of GlOH and consequently problems in distributing the substance excess. Therefore, GlOH has been considered as a potential feedstock for new industrial applications such as the production of more valuable fine chemicals as dihydroxyacetone, glyceric and hydroxypyruvic acids, 1,2- and 1,3-propanediol, and propylene glycol[1−5] or in direct use as a fuel in fuel cells.[6]

However, the main practical difficulty is to selectively produce the desired product from GlOH oxidation, preferably under mild conditions without the use of chromates, permanganates, or hypochlorites, which generates industrial waste. In this context, the partial electrochemical oxidation of GlOH on noble-metal-based materials seems to be a promising route to overcome this problem.

Received: March 3, 2015
Revised: May 11, 2015
Published: May 28, 2015

DOI: 10.1021/acscatal.5b00451
ACS Catal. 2015, 5, 4227−4236

Accordingly, substantial effort has been devoted to understanding the glycerol electro-oxidation reaction (GEOR) and the effect of the variables involved in this process.

Kwon and co-workers[7] showed that gold catalyzes GlOH oxidation only under alkaline conditions, in contrast to platinum, which catalyzes GlOH oxidation over the entire pH range. In addition to the role of the metal's nature, special attention has been paid to the cation influence on the kinetics of GEOR in alkaline media, showing that noncovalent interaction between hydrated alkali-metal cations and OH_{ad} is present on Pt but absent on Au. Fernandez et al.[8] studied the GEOR using in situ FTIR and isotopically labeled GlOH. The results indicated the presence of CO_2 as a reaction product, implying that GlOH dissociates on Pt surfaces and that C−C bonds can be broken. Studies using density functional theory (DFT) reported that GlOH interacts with the platinum surface via hydroxyl groups,[9,10] and the interaction of the OH groups with Pt surfaces affects the atomic structure of GlOH in comparison with the gas phase: in particular, the orientation of the OH groups with respect to the C−C bonds.[11]

In a recent voltammetric study of GEOR on Pt single crystal, it was concluded that the reaction is highly dependent on the surface site orientation. At low potentials, Pt(111) is more active for GlOH electro-oxidation than Pt(100) and Pt(110);[12] as seen by in situ FTIR spectroscopy, the reason may be that carbon monoxide, a common adsorbed intermediate of organic molecule oxidation on Pt, was more easily removed from Pt(111) than from Pt(100) and Pt(110).[13] These results obtained on well-ordered surfaces follow the trend of structure sensitivity of most electrochemical reactions, namely hydrogen,[14] carbon monoxide,[15] methanol,[16] ethanol,[17] and ethylene glycol[18,19] oxidation and oxygen[20] and nitrate[21,22] reduction, among others.

In this way, the relationship between the different site symmetries at the electrode surface and its response provides a powerful tool for designing nanocatalysts for practical uses.[23−25] Therefore, the use of well-ordered surfaces to understand the key role played by the surface structure underwent great improvement after the publication of the "flame annealing method" by Clavillier et al.[26] The presence of dilute defects on single-crystal surfaces, known as stepped surfaces, allows the systematic study of the influence of well-defined defects in different systems. The usual approach is to begin with a very well-ordered surface, without defects, and proceed toward more complex systems using stepped surfaces with different quantities of a given defect (steps or kinks at different surface geometries), providing a decrease of terrace domains as the number of defects increases.

Despite these advances and some insights published in our previous work,[12] it remains unclear how the nature and quantity of surface defects influences the GEOR. For this investigation, we electrochemically generate a set of Pt(100) surfaces with a controlled density of defects and with diverse defect symmetry. This strategy presents a new path to linking well-ordered with disordered surfaces, using a set of surfaces with nondefined defects (in contrast to the well-defined defects of the stepped surfaces). It is a highly reproducible method and could be potentially applied to other systems, not necessarily just electrochemistry.

Then, with the aim of understanding the GEOR mechanisms on platinum at different degrees of surface order, moving from an ideally ordered to a highly disordered surface and hence approaching the highly disordered real systems, we used the electrochemically generated disturbed surfaces to study the GEOR. Conventional techniques such as CV and FTIR were combined with DFT. The results showed that the disturbed surfaces are poorer catalysts than the well-ordered Pt(100) single crystal; this appears to be connected with the stronger Pt−CO bonding on the low-coordinated Pt atoms of disturbed surfaces.

EXPERIMENTAL SECTION

Electrochemical Systems and Spectroelectrochemical Experiments. All of the experiments were performed at room temperature (25 ± 1 °C) in a conventional three-electrode electrochemical cell. A high-area polycrystalline Pt sheet was used as a counter electrode. The reference electrode was a reversible hydrogen electrode (RHE). The working electrode was a 1 cm diameter Pt(100) disk acquired from MaTeck.

In order to check the platinum surface order, cyclic voltammograms (CVs) were obtained in the potential range between 0.05 and 0.80 V in a 0.5 M H_2SO_4 solution. The solution cleanliness was checked by the stability of the voltammetric features of Pt electrodes. The upper potential limit was set to avoid any Pt oxide formation, which generates irreversible surface disordering.

The FTIR instrument was a Nicolet Nexus 670 spectrometer equipped with a liquid-nitrogen-cooled MCT detector. In situ FTIR experiments were performed in a three-electrode spectroelectrochemical cell with a planar CaF_2 window attached to the bottom of it. Details concerning the cell are described elsewhere.[27] Briefly, a movable piston supports the working electrode. A Pt wire connected to the working electrode passes through the piston and maintains the electrical contact. The CaF_2 window functions as a transparent cell bottom and as a wall against the working electrode. It is pressed to obtain a thin film of electrolytic solution. In this way, the absorption of the infrared beam by the solution is minimized during the FTIR measurements.

The FTIR spectra were computed from an average of 128 interferograms. The spectral resolution was set to 4 cm^{-1}. First, the working electrode was placed in the meniscus configuration, and five consecutive CVs were obtained in a solution of 0.2 M GlOH and 0.5 M of H_2SO_4. The potential was kept at 0.12 V, and the electrode was dipped in the solution until it contacted the window. When the system became stable (the recorded spectrum did not change with time at 0.12 V and was set as reference spectrum), a linear potentiodynamic sweep was started at 0.002 V s^{-1}, and the scan was stopped every 0.005 V for enough time to obtain 128 interferograms (approximately 1 min). Thus, the first spectrum was obtained at 0.15 V, the next at 0.20 V, and so on until 0.95 V. The choice of this upper potential limit will be explained below.

Working Electrode Surface Preparation. To obtain perfectly ordered and clean surfaces, the working electrode was flame-annealed in a butane−oxygen flame for 1 min and cooled under a reductive H_2 + Ar atmosphere for 5 min. The electrode surface was then protected with a water droplet saturated with cooling gases to prevent contamination and reconstruction of the surfaces during the transfer to the electrochemical cell.

To monitor the influence of the upper potential limit on the Pt(100) surface order degree, the potential limit was progressively augmented from 0.80 V until 1.05 V. Through this experiment, we determined that (i) the Pt(100) surface cycled until 0.95 V remains unchanged and very well ordered (at least for some cycles) and (ii) cycling up to 1.05 V

DOI: 10.1021/acscatal.5b00451
ACS Catal. 2015, 5, 4227−4236

progressively generates more and more disordered Pt(100) surfaces. This limit is low enough to permit surface order monitoring (through some characteristic voltammetric features that are discussed later) and thus gives the possibility of stopping the experiments after obtaining a surface with the desired defect density. The incursion in higher potentials (above 1.05 V) can cause severe surface disordering even in the first cycle.[28] After this experiment, the upper potential limit was set at 0.80 V again to obtain a CV of the modified Pt(100) surface (blank CV) for direct comparison with the very well-ordered Pt(100) surface.

In this work, five different disordered Pt(100) electrodes were obtained. In ascending order of defect density, they are as follows (the different electrode names Pt*X*-*Y* will be explained later): (i) Pt0-100, perfectly ordered surface; (ii) Pt25-75, surface obtained after 4 CVs up to 1.05 V; (iii) Pt50-50, surface obtained after 8 CVs up to 1.05 V; (iv) Pt75-25, surface obtained after 16 CVs up to 1.05 V; (v) Pt100-0, surface obtained after 25 CVs up to 1.05 V + 12 CVs up to 1.20 V. In this last case, the potential limit was changed to obtain a completely disordered Pt(100) surface.

Once the desired surface was prepared, the platinum surface order was checked again by measuring CVs in the potential range between 0.05 and 0.80 V in a 0.5 M H_2SO_4 solution. Then, it was protected with an electrochemical solution droplet and transferred to another identical electrochemical cell containing a 0.5 M H_2SO_4 and 0.2 M GlOH solution. The Pt(100) surface was placed in contact with the solution at 0.12 V in all experiments. This potential was chosen to minimize Faradaic processes other than GlOH dissociative adsorption.[29]

Theoretical Approach and Computational Details. We investigated the structural and energetic properties of GlOH and carbon monoxide (CO) on the Pt(100) surface using DFT within the generalized gradient approximation proposed by Perdew–Burke–Ernzerhof (PBE)[30] for the exchange-correlation (xc) energy functional. To solve the Kohn–Sham equations, we employed the Vienna ab initio simulation package (VASP)[31,32] with the all-electron projected augmented wave (PAW) method implemented[33,34] and the PAW projectors to describe the electron–ion interactions. For all of the total energy surface calculations, a plane-wave cutoff energy of 487 eV was used, whereas for the integration of the Brillouin zone (BZ), a 3 × 3 × 1 *k*-point mesh was used. We obtained the equilibrium atomic positions once the atomic forces on each atom were smaller than 0.025 eV/Å with a total energy convergence of 10^{-5} eV.

The unreconstructed Pt(100) surface was obtained using a periodic surface slab model with a thickness of six layers with a (4 × 4) surface unit cell (16 Pt atoms per plane) and a 20 Å vacuum region. The defected Pt(100) surface was modeled based on the unreconstructed Pt(100) surface model where 10 surface atoms were removed and the remaining 6 atoms on the surface have lower coordination; thus, this surface has fewer coordinated sites and terraces (this surface will be termed Pt_6/Pt(100) in our discussion to differentiate it from the electrochemically prepared disordered surfaces). The molecules adsorbed only on one side of the slab. Only the bottom layer of the slab was frozen, while the other five layers along with the adsorbates were allowed to relax in all calculations.

To study the complicated structure of the CO-GlOH mixture on the disordered Pt(100) surface, i.e., Pt_6/Pt(100), we searched for the lowest energy configurations by performing the following steps. (i) Several initial configurations were presented with three CO molecules initially adsorbed at the different positions on the unreconstructed Pt(100) surface, i.e., top, bridge, and hollow sites and their combinations, to identify the correct adsorption site on the clean Pt(100) surface. The knowledge of the adsorption site preference was used in the next steps of the simulations. (ii) We then modeled the configurations in which CO molecules were located on the lower and higher coordinated sites of the Pt_6/Pt(100) surface, i.e., terraces and islands, and their combination. (iii) We simulated GlOH adsorption on our surfaces. It is important to note that, in our previous work, we carefully investigated GlOH configurations on Pt(*hkl*) surfaces using ab initio molecular dynamics simulations and found the lowest energy configuration for GlOH on Pt(100).[11] We revealed that GlOH binds with the Pt(100) surface with an adsorption energy of −0.44 eV via the O atom, where the distance between the O and Pt atoms is 2.45 Å and the angle between the bonds of the edge C atoms and the surface normal is 79.46°. In this work, employing the GlOH structure on the previously obtained clean Pt(100) surface,[11] we modeled different atomic configurations of GlOH on the Pt_6/Pt(100) surface, where GlOH adsorbed on the lower coordinated sites and on the terraces. (iv) Complex systems consisting of three CO molecules and GlOH on the Pt_6/Pt(100) surface were simulated using the lowest energy structure of GlOH on the Pt_6/Pt(100) surface, in which CO molecules were bound on different positions of the surface: i.e., the lower coordinated sites and the terraces. All structures were optimized employing the standard VASP optimization procedure.

To analyze the lowest energy structures, we computed adsorption energies by applying the following formulas: $E_{ad} = E^{tot\text{-}system} - (3{*}E^{CO} + E^{clean\ Pt})$ for 3 CO, $E_{ad} = E^{tot\text{-}system} - (E^{GlOH} + E^{clean\ Pt})$ for GlOH, and $E_{ad} = E^{tot\text{-}system} - (3E^{CO} + E^{GlOH} + E^{clean\ Pt})$ for the GlOH and 3 CO mixture on the Pt surface. Here, $E^{tot\text{-}system}$, E^{CO}, E^{GlOH}, and $E^{clean\ Pt}$ are the total energies of the system, CO and GlOH molecules in the gas phase, and the clean Pt surface, respectively.

RESULTS AND DISCUSSION

Pt(100)-Modified Electrodes. TEM and STM are typical ex situ characterization techniques. The former is very useful for identifying the size and shape of nanomaterials, whereas STM can provide valuable information on the surfaces. However, these techniques are time-consuming and expensive, and they provide only local information. Sometimes, even by taking images of an important quantity of different surface regions, it is impossible to extrapolate the results to the whole electrode surface. In this context, surface characterization techniques in the metal–solution interface are well-established as the best tools to monitor the different symmetry sites in this type of system, providing us an overall response of the surface in contact with the electrochemical solution. Thus, the so-called hydrogen adsorption/desorption region is very useful for qualitative characterization of the Pt surfaces.[23,28,35−37] In this way, the CV profile for the platinum electrode is considered a fingerprint of the surface structure, giving us information about the symmetry and distribution of the surface sites, as well as the system's general conditions and cleanliness. Therefore, our starting point in this work was to analyze the electrode surface structure from the density current response displayed in the CVs recorded only in the presence of the sulfuric acid.

Figure 1 (black line) shows the blank CV of a well-ordered Pt(100) electrode. The profile presented is consistent with

DOI: 10.1021/acscatal.5b00451
ACS Catal. 2015, 5, 4227−4236

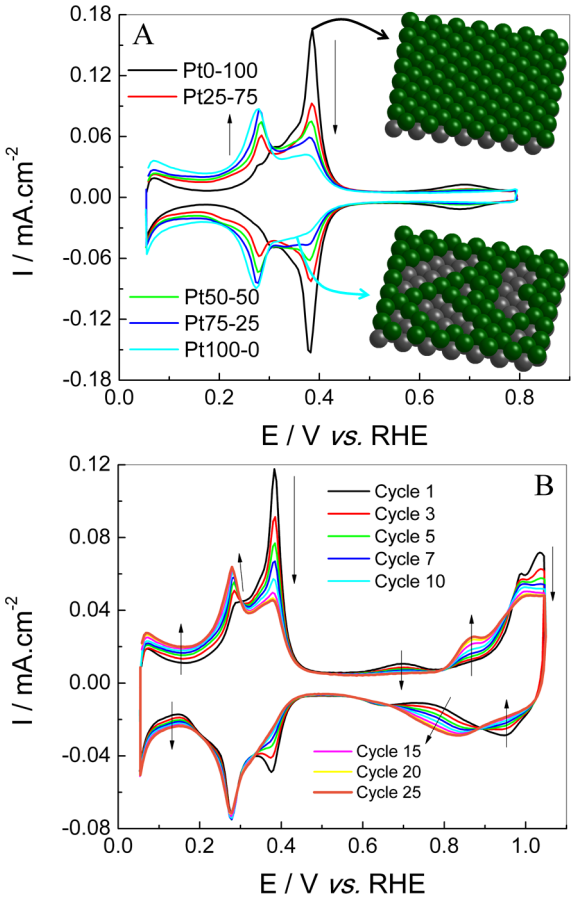

Figure 1. (A) Voltammograms obtained in 0.5 M H_2SO_4 solution for the different defect density Pt(100) surfaces. The black CV shows the typical electrochemical features of an ordered Pt(100) surface, and the light blue CV corresponds to a highly and randomly disordered surface. (B) Generation of disordered electrode by cycling up to 1.05 V. ν = 0.05 V s^{-1}.

other published results, characterized by a narrow peak at 0.37 V with a symmetrical density current in the positive and negative scan.[38] Any surface structure modification leads to a change in the CV profile. Specifically for Pt(100) electrodes, changes can be easily identified by (i) decreases in the characteristic peak at 0.37 V, (ii) the appearance of a peak at 0.26−0.28 V, and (iii) increases in the density current below 0.20 V, as seen in Figure 1A for the Pt25-75, Pt50-50, Pt75-25, and Pt100-0 electrodes. The current signals at 0.26−0.28 V and below 0.20 V were previously assigned to hydrogen adsorption/desorption on border or step sites with the (110) and (111) orientations, respectively.[35,38,39]

The terminology Pt*X*-*Y* refers to the intensity of the peak at 0.26−0.28 V (*X*) and of the peak at 0.37 V (*Y*). Pt0-100 stands for the perfectly ordered Pt(100) surface. The corresponding CVg presents only the peak at 0.37 V (Y). Consequently, for Pt0-100, *X* = 0 and *Y* = 100. Pt50-50 represents the surface presenting features at 0.26−0.28 V (*X*) and 0.37 V (*Y*) with approximately the same intensity. Pt100-0 represents the totally disordered Pt(100) surface, for which the corresponding CVg presents only the peak at 0.26−28 V. Pt25-75 and Pt75-25 are electrodes presenting fewer and more defective surfaces than Pt50-50, respectively.

To achieve systematically different surface electrode configurations and study the influence on GlOH oxidation, we applied successive cycles on the Pt0-100 electrode up to 1.05 V, keeping the lower potential at 0.05 V. Figure 1B shows the surface modification during 25 consecutive CVg. These 25 CVg are only applied to obtain the Pt100-0 surface. When a more ordered surface is desired, for instance, the Pt50-50 electrode, the cycling until 1.05 V is stopped after the fourth cycle and the blank CVg is recorded again. Thus, the electrochemical features of the disturbed electrodes (blank CVg) after the surface modification procedure are displayed in Figure 1A. (Figure S1 in the Supporting Information shows the complete cycling for the generation of Pt100-0).

It is well-known that the excursion into the oxygen adsorption region causes intense surface structural modification.[40] In Figure 1B, the evolution of the continuous cycling is characterized by changes in the hydrogen adsorption/desorption region (E < 0.4 V) and the appearance of a redox response at potentials above 0.80 V. The formation of a submonolayer oxide film, recognized as OH and O electrosorption,[41] leads to a progressive and irreversible transformation of a well-defined 2-D surface to one in which the local order is continuously changed by covering the surface with defects. Such defects can be assigned as single adatoms, small islands, pits, or other collections of defects, as described by Björling and Feliu[42] for a series of experiments in the study of oxide formation on Pt stepped surfaces. In addition to the changes in the hydrogen adsorption region, the appearance of defect sites/domains on the surface leads to hysteresis in the current response during the anodic oxygen adsorption and cathodic reduction of the oxide film.

The CVg of the electrochemically disordered Pt100-0 electrode indicates that the surface retains the symmetry of the (100) sites, but with a depletion of the large domains with an increase of the cycles into the oxygen adsorption region. The quantification of the actual (100) terrace sites at every modified electrode is not a simple assignment determined solely by the analysis of the blank CVg. Solla-Gullón et al.[43] proposed a quantitative method for the estimation of surface sites on Pt samples using specific site-probe reactions. However, in this work, we achieved the presence of the (100) domains and the surface defects influence on the GEOR without a quantitative estimation of the specific surface orientation. On the other hand, the "soft" damage caused by cycling into the early stages of oxygen adsorption potentials showed that we can produce a surface with a systematic decrease of large terrace domains.

At this point in the work, it is interesting to clarify the differences in surface structures presented in a model single-crystal electrode produced with systematic density defects (stepped surfaces) and those produced in this work. Although the CV profiles of Pt stepped surfaces are highly similar to those displayed here, the assignment of the specific kind of defect (kinks and steps), as well as the terrace width distribution, on Pt(100) modified electrodes is not straightforward without their characterization by additional techniques[42,44] and experiments.

GlOH Electrooxidation on Pt(100) Surfaces. Parts A and B of Figure 2 show five consecutive CVg for Pt0-100 and Pt100-0, respectively. The CV features for the GEOR change progressively from the well-ordered surface, Pt0-100, to the totally disturbed one, Pt100-0. Thus, for the sake of clarity, we decided to present the two limit behaviors (Figure S2 in the Supporting Information shows the Pt50-50 behavior).

In general, the first CV for the GEOR on Pt0-100 and Pt100-0 presents current signals at 0.20−0.70 V and a sharp oxidation

DOI: 10.1021/acscatal.5b00451
ACS Catal. 2015, 5, 4227−4236

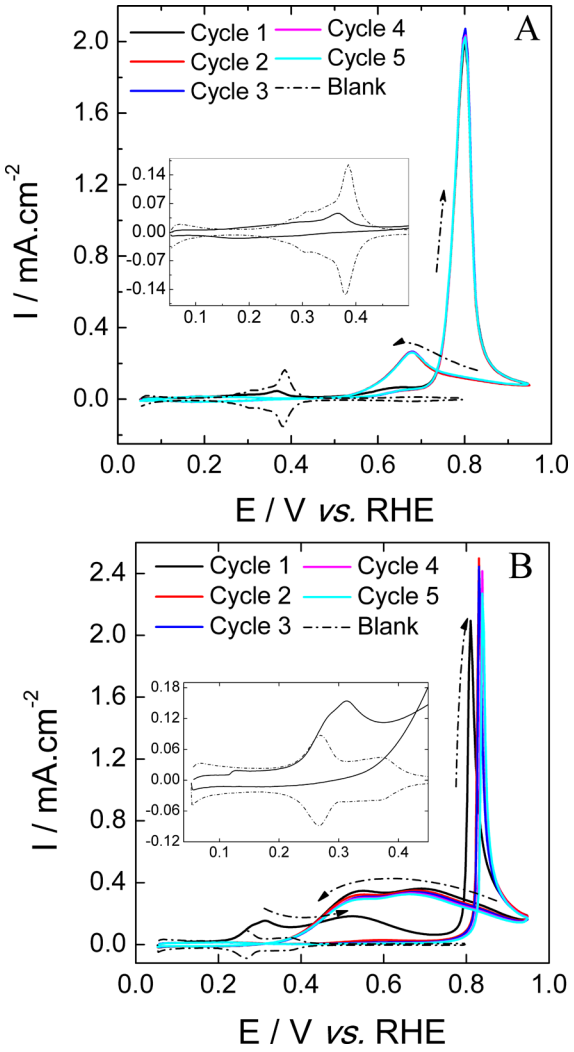

Figure 2. Voltammograms obtained in 0.2 M GlOH and 0.5 M H_2SO_4 solution with Pt0-100 (A) and Pt100-0 (B). ν = 0.05 V s^{-1}.

peak close to 0.80−0.85 V in the positive-going potential scan and a reactivation wave between 0.95 and 0.4 V in the negative-going potential scan. Remarkably, as the density of defects increases, the sharp oxidation peak in the positive scan becomes thinner. The current signals at 0.20−0.70 V vanish from the first to the second CVg for both electrodes. From the second to the fifth CVg, the changes are not significant, especially for Pt0-100. After the fifth potential cycle, the changes in the CV profile for both electrodes become negligible.

As mentioned above, the main difference between the first and the subsequent CVg is the presence of current signals between 0.20 and 0.70 V, which are present only at the first potential cycle. These current signals are related (at least in part) to GlOH and hydrogen/anion coadsorption, as seen in the insets in parts A and B of Figure 2, and the lack of them from the second potential cycle on demonstrates that the adsorption layer formed at 0.12 V when the electrode is put in contact with the solution is clearly distinct from the adsorption layer formed at the beginning of the second CVg after the excursion to higher potentials. In particular, the absence of any current signal between 0.20 and 0.70 V indicates that the surfaces are completely blocked by the adsorption of GlOH or its derivatives in this potential region.

Detailed analysis of the first CVg (parts A and B of Figure 2) reveals important differences between the GEOR on Pt0-100 and Pt100-0. In the positive-going potential scan, while the perfectly ordered surface shows a small peak in the coadsorption region and a prewave before the main oxidation peak, the totally disturbed surface presents important oxidation peaks from 0.2 to 0.95 V. Therefore, the defects favor the oxidation of the GlOH residues at low potentials in the first positive-going potential scan. Interestingly, in the next scans, when the surfaces are completely blocked at lower potentials, the defects act in a contrary manner, increasing the potential needed to oxidize the GlOH molecules and/or their derivatives, as seen by the potential of the sharp peak, which is higher for Pt100-0 than for Pt0-100. These results show that the defects strongly influence the surface responses in the positive-going potential scan.

In addition, in the negative-going potential scan, the CV profile of the reactivation wave also depends on the density of the surface defects. For Pt100-0, this signal shows at least two different contributions. The first peak is centered at approximately 0.70 V and the second peak at approximately 0.50 V. The peak at 0.70 V coincides with that for Pt0-100. This result suggests that this contribution is connected to extended well-ordered surfaces and that located at lower potentials appears to be connected with the reactivation of the disordered domains.

To further evaluate the impact of the surface defects on GEOR over modified Pt(100), the onset potential and the potential of the sharp peak were extracted from the fifth positive-going potential scans (shown in parts A and B of Figure 2) and plotted as a function of the density of surface defects. These data are presented in Figure 3. Figure S3 in the Supporting Information shows the process used to calculate the onset potential for every electrode.

Figure 3A shows a continuous displacement of the onset potential toward more positive potentials with increasing

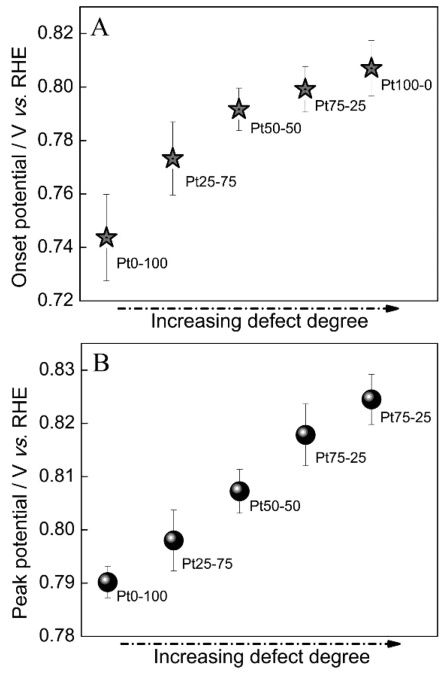

Figure 3. Changes in the onset potential (A) and in peak potential (B) of the GEOR as a function of the degree of electrode defects.

DOI: 10.1021/acscatal.5b00451
ACS Catal. 2015, 5, 4227−4236

density of surface defects. In particular, from the perfectly ordered surface to the totally disordered surface, the onset potential shifts by approximately 100 mV (Figure 3A), which is a significant change in terms of energy. The potential of the sharp peak follows the same trend as a function of the density of surface defects (Figure 3B), although it is less sensitive to the presence of defective sites than the onset potential. Therefore, these results clearly demonstrate that under steady-state conditions (at the fifth CVg), as the density of surface defects increases, more energy is necessary to oxidize GlOH and its derivatives.

Returning to Figure 1B, we see that the continuous defect generation produces a displacement of the oxide formation domain to lower potentials. It is generally accepted that the onset potential of the oxidation of small organic molecules is connected to the Pt−OH formation. Thus, the Pt−OH species react with the preadsorbed molecules (generally through a Langmuir−Hinshelwood mechanism), producing several products and thus generating positive currents. As we previously showed, our results are not consistent with this idea, as we observed an increase in onset potential for electrodes that form Pt−OH at lower potentials. Clearly, this description is an oversimplification of a very complicated system, where water, anions, cations, and organic molecules compete at different potentials, sometimes for a myriad of diverse Pt adsorption sites (where diverse adsorption sites imply different site configurations and adsorption energies).

FTIR in Situ Experiments. Figure 4 shows some selected spectra obtained with Pt0-100 and Pt100-0. In Table S1 in the Supporting Information, the main band assignments can be observed. A band centered at 2343 cm^{-1} corresponding to the asymmetric stretching of CO_2 is present for both surfaces. Additionally, a band centered at 2040 cm^{-1}, whose frequency varies with the working electrode (the frequency variation is shown in Figure S4 in the Supporting Information), is attributed to the on-top bonded CO and is also present for both surfaces. Another very important feature at approximately 1740 cm^{-1} corresponding to carbonyl-containing compounds (C═O) can be observed in Figure 4, and a detailed inspection of this band shows that it consists of at least two superimposed signals (see Figure S5 in the Supporting Information). Again, this signal is also present for both surfaces. Finally, at least three bands between 1100 and 1300 cm^{-1} can be observed. Briefly, they correspond to the generation of carboxylic acids, the consumption of GlOH, and the entrance of SO_4^{2-} and HSO_4^- ions in the thin layer during the potential scan. Unfortunately, the signal of the anions (both those in the solution and those bound to Pt) is too strong to permit a clear observation of other interesting signals present in the same wavenumber domain. The same general features were previously observed by Gomes et al.[13]

Figure 5 reveals details of the bands in the wavenumber region between 2100 and 1800 cm^{-1}. For Pt0-100, a positive band located at approximately 1870 cm^{-1} corresponding to bridge-bonded CO is seen from 0.30 V on. In contrast, for Pt100-0 a negative band at approximately 1840 cm^{-1} with a very low intensity also corresponding to bridge-bonded CO can be seen. These results clearly indicate that bridge-bonded CO was already present at the beginning of the experiment at 0.12 V for Pt0-100 but not for Pt100-0.

The behavior of the bands corresponding to on-top bonded CO, CO_2, and C═O formation (shown in Figure 4) as a function of the electrode potential is further evaluated in Figure 6. To construct this figure, CO and CO_2 bands were integrated along the potentiodynamic sweep. As the C═O band superimposes with a broad positive band at 1630 cm^{-1} due to the continuous exit of water from the thin layer, the C═O band area is not clearly defined and for this reason could not be integrated. To quantify the production of C═O-containing compounds, we measured the variations in peak intensity with respect to a baseline passing through the left queue of the C═O band, at the opposite side of the water band (Figure S6 in the Supporting Information).

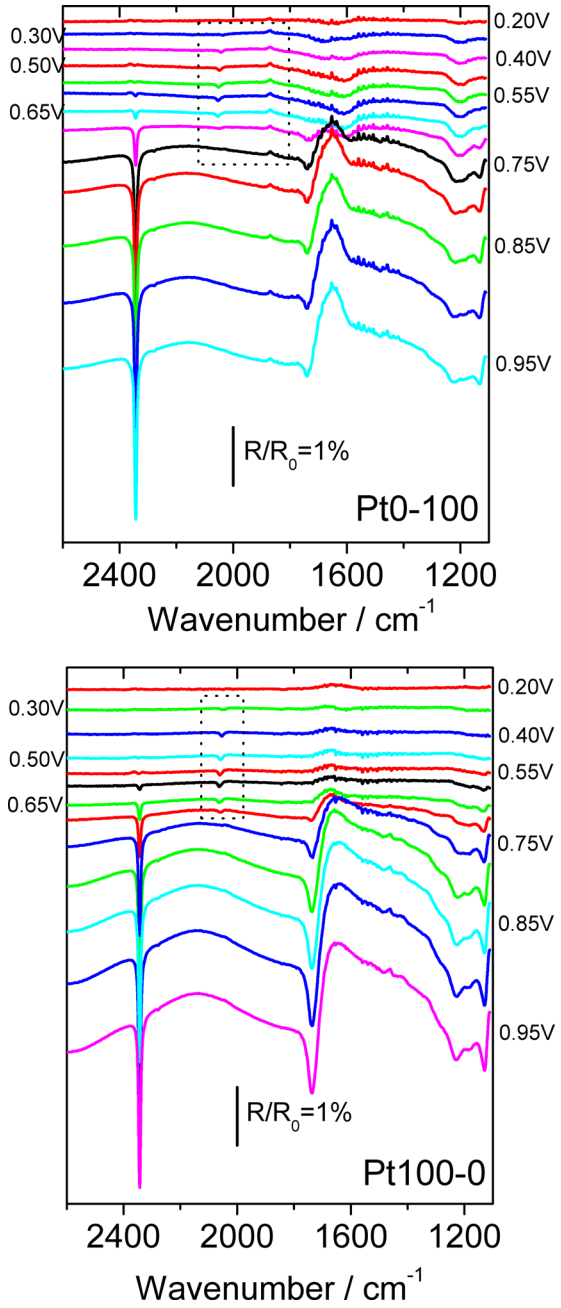

Figure 4. Selected FTIR spectra obtained at different working electrode potentials in 0.2 M GlOH + 0.5 M H_2SO_4. Spectra obtained at lower potentials do not show any important difference with respect to the background spectra obtained at 0.12 V.

As seen in Figure 6, CO is formed on Pt0-100 and Pt100-0 at low potentials (the first discernible signal appears at 0.30 V), and its production increases continuously until attaining a

DOI: 10.1021/acscatal.5b00451
ACS Catal. 2015, 5, 4227−4236

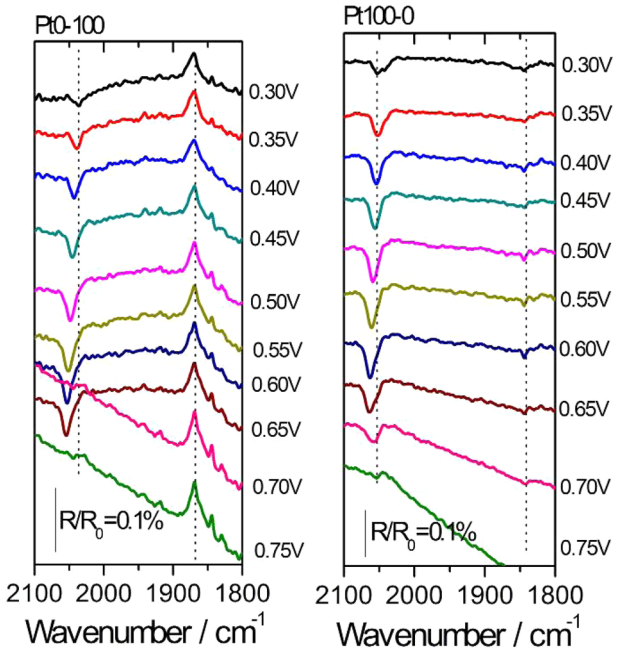

Figure 5. Enlarged view of the rectangular region of Figure 4 drawn with dashed lines. Both surfaces show signals attributed to top- and bridge-bonded CO.

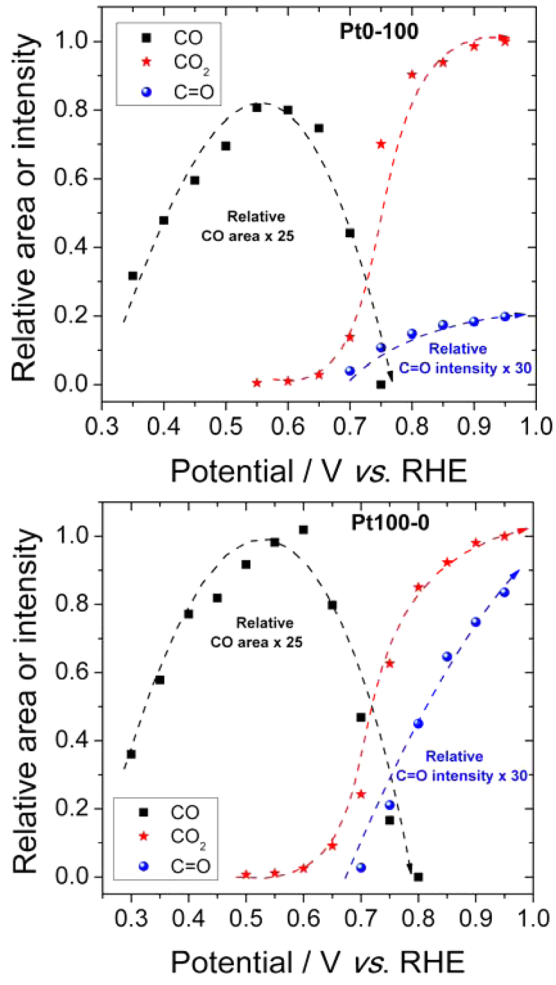

Figure 6. Intensities of C═O and absorbances of on-top bonded CO and CO_2. Both intensities and absorbances were divided by the corresponding maximum CO_2 band absorbance, i.e., the CO_2 band integration value obtained at 0.95 V. Figure S7 in the Supporting Information shows the crude results for two independent measurements.

maximum at approximately 0.60 V, when it suddenly decreases. This abrupt decrease occurs in the same potential domain where the CO_2 formation increases quickly. It is reasoned to be a consequence of the oxidation of GlOH to CO_2, with CO as a reaction intermediate. Interestingly, the amounts of on-top bonded CO with respect to CO_2 are fairly different for Pt0-100 and Pt100-0, being higher for the disordered surface, suggesting that Pt100-0 exhibits greater ability in C−C bond breaking and converting CO into CO_2. On the other hand, for Pt0-100, CO_2 may be formed in part through a pathway that does not involve CO as an intermediate. The behavior of the on-top bonded CO and CO_2 formation is very similar to the behavior found by our group in previous works.[8] The development of these species on the Pt100-0 surface is shown in this work for the first time.

A very interesting result is that C═O formation was observed from 0.70 V on both surfaces: that is, 0.10 V after beginning the CO oxidation. This result suggests that GlOH and CO compete for catalytic sites, with CO being the main adsorbate at low potentials, whereas GlOH can massively adsorb at relatively high potentials to produce CO_2 through a direct pathway or be oxidized to form C═O with or without C−C bond breaking (the main C═O signals observed for polycrystalline Pt in the same potential domain used in this work come from glyceraldehyde and glyceric acid[7]).

By a comparison of the ratio between C═O and CO_2 produced on Pt0-100 and Pt100-0, a very important observation arises from both the basic and applied perspectives. On the disturbed surface, the formation of carbonyl-containing compounds increases rapidly and continuously along the potential scan, whereas on the well-ordered surface, the signal changes only slightly between 0.80 and 0.95 V. For example, at 0.95 V, the ratio between C═O and CO_2 formed on the disturbed surface is approximately 6 times higher than that on the well-ordered surface. This difference is important and might be useful from a technological perspective. This type of experiment may serve as a starting point for the selective production of C═O GlOH derivatives, assisting in the choice of an appropriate real catalyst (e.g., nanomaterials) with a suitable shape for the production of GlOH derivatives with added value.[45,46]

Density Functional Theory Calculations. To gain further insight into the GEOR, we performed computational calculations including modeled well-ordered and disordered Pt(100) surfaces. In addition, the stability of these systems in the presence of CO, GlOH, and CO + GlOH was carefully studied.

Structural and Adsorption Properties. The lowest energy configurations for 3 CO, GlOH, and the 3CO + GlOH mixture on the Pt(100) and Pt_6/Pt(100) surfaces are shown in Figure 7. High-energy isomers are shown in Figures S8−S11 in the Supporting Information. We found that CO molecules bind to the Pt(100) surface via C atoms on the bridge sites and that moving one of the CO molecules to the on-top site of Pt(100) increases the total energy of the system by 0.25 eV (Figure S8). On the Pt_6/Pt(100) surface, we observed that all of the CO molecules prefer binding on the low-coordinated Pt_6 atoms (Figure 7). We expected from the CO/Pt(100) calculations that all of the CO molecules would

DOI: 10.1021/acscatal.5b00451
ACS Catal. 2015, 5, 4227−4236

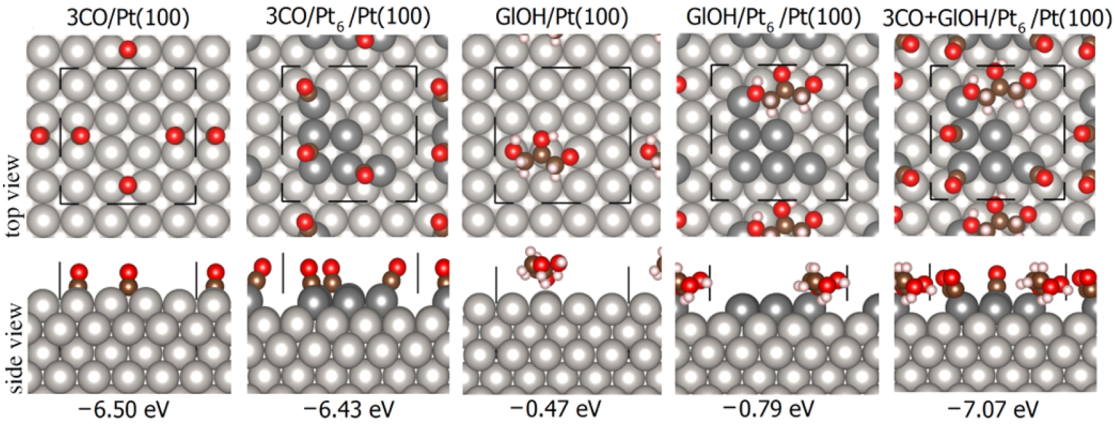

Figure 7. Lowest energy configurations for all of the systems and their adsorption energies.

be located on the bridge sites; however, we found that only two molecules are located on the bridge sites of the low-coordinated Pt_6 atoms, whereas one CO adsorbs on-top of the edge low-coordinated Pt_6 atom due to the release of the strain from the molecular repulsion. The configuration in which all CO molecules bind on bridge sites of Pt_6 is only 0.16 eV higher in energy than the lower energy configuration, which means that this configuration might exist under certain experimental conditions: e.g., in high-temperature experiments. Surprisingly, the adsorption of CO is slightly stronger on Pt(100) than on the Pt_6/Pt(100) surface (by 0.07 eV), considering the presence of the low-coordinated atoms on Pt_6/Pt(100). The given quantity of CO molecules (i.e., three molecules) was chosen by us for our DFT calculations in order to take into account the intermolecular interaction and binding of CO molecules on different surface adsorption sites. In our lowest energy structures CO molecules bind at both top and bridge sites, as supported by our spectroelectrochemical experiments, which implies that the quantity of CO molecules chosen for our DFT calculations is feasible, taking into account the size of the unit cell.

In the lowest energy structure of GlOH on Pt(100) obtained in our previous work,[11] we revealed that GlOH binds with the Pt(100) surface with an adsorption energy of −0.44 eV via the O atom, where the distance between the O and Pt atoms is 2.45 Å and the angle between the bonds of the edge C atoms and the surface normal is 79.46°. In the lowest-energy atomic structure of GlOH on the Pt_6/Pt(100) surface, the GlOH molecule favors binding on the triangle low-coordinated Pt_6 edge atom, whereas its total energy is 0.32−0.54 eV higher in the terraces (see configurations E−G in Figure S10 in the Supporting Information). The lowest energy structure of GlOH on Pt_6/Pt(100) is modified by comparison with GlOH on Pt(100),[11] i.e., the O−Pt bond lengths are 2.32 and 2.21 Å, and the angles between the C−C bond and the normal to the surface are 78.55 and 90.39° on the Pt(100) and Pt_6/Pt(100) surfaces, respectively, implying stronger binding with the low-coordinated Pt_6 atoms, which is reflected in the adsorption energies, i.e. −0.45 and −0.79 eV, respectively.

The structure of the mixture of 3CO and GlOH molecules on Pt_6/Pt(100) (Figure 7 and Figure S11 in the Supporting Information) presents all of the molecules located on the low-coordinated atoms Pt_6, in which the GlOH geometry is modified only slightly on the surface in comparison with GlOH/Pt_6/Pt(100): i.e., binding to the edge Pt atom with an O−Pt bond length of 2.19 Å and C−C−normal angle of 89.45°. Here, all of the CO molecules bind to the on-top sites of Pt_6, a preference that can be explained by the intermolecular repulsion. Moving CO molecules to the terraces of Pt(100) increases the total energy of the system (see configurations B−D with their relative total energies of 0.07, 0.22, and 0.92 eV, respectively, in Figure S9 in the Supporting Information). The adsorption energy for 3CO + GlOH/Pt_6/Pt(100) is slightly smaller (−7.07 eV) than that obtained if we sum up the separate systems, i.e., (−6.43 + −0.79 = −7.22 eV), which implies an intermolecular interaction.

To obtain a better understanding of the binding mechanism between the molecules and the defected Pt_6/Pt(100) surface, we calculated the following properties of the systems: local density of states, the changes in the substrate work function, which reflects electron density rearrangement on the surfaces upon the adsorption of molecules, and an effective charge of every atom on the systems using Bader charge analysis. All of these properties are discussed in the Supporting Information section.

DFT Calculations and Electrochemical and Spectroelectrochemical Experiments. We have shown in Figure 3 that the GEOR onset potential displaces toward positive potentials as the density of surface defects increases. We noted that this result does not agree with the fact that disturbed electrodes form Pt−OH species at lower potentials in comparison to Pt(100), which would permit Pt−OH and Pt−GlOH* (GlOH* = GlOH or GlOH residues) combination at lower potentials. On the other hand, the DFT calculations show that both CO and GlOH bind more strongly to the low-coordinated Pt sites on the surface with defects. Therefore, the increase of the GEOR onset with increasing density of surface defects is probably because GlOH (and CO, which remains the only detected intermediate, although the presence of other species is probable, as noted during the discussion of Figure 2) binds more strongly on these surfaces, indicating that the residue detachment is the rate-determining step of the GEOR.

Interestingly, FTIR data showed that the presence of superficial defects on Pt favors GlOH C−C bond breaking, which seems to be connected (among other factors) with the surface ability to attach GlOH through at least two oxygen (or carbon) atoms. Correspondingly, DFT shows that GlOH attaches to a well-ordered Pt(100) surface and to a disordered surface at angles of approximately 21 and 10°, respectively, with respect to the surface. Most likely, the lower angle between GlOH and the disturbed surface favors the molecule's

DOI: 10.1021/acscatal.5b00451
ACS Catal. 2015, 5, 4227−4236

attachment through multiple atoms, facilitating C−C bond breaking.

Figure 6 shows that, on both surfaces, GlOH adsorption and oxidation occurs (or is detected) after the beginning of the on-top CO oxidation. The DFT results show that the CO−Pt bonds (on bridge and on-top positions) are much stronger than on-top GlOH−Pt bonds for both surfaces: that is, in high-coordinated as well as in low-coordinated Pt atoms. As a consequence, regardless of the exact nature of the early adsorbate, the generation of CO through the GlOH dissociative adsorption at low potentials does not permit detectable GlOH adsorption and further oxidation. In other words, the Pt−GlOH interaction is not strong enough to withdraw CO from the surface. This fact again suggests that the GEOR is mainly determined by the strength of the GlOH*−Pt bonds.

Finally, at high potentials (>0.80 V), where the GlOH molecule is easily oxidized, we showed that the C═O production is high on Pt100-0 and negligible on Pt0-100. Although more DFT calculations are needed, the computational simulations showed that the GlOH−Pt bond strength is larger for the low-coordinated Pt atoms. Perhaps in this potential domain the GEOR to C═O is determined by the GlOH surface attachment rate, and this reaction step depends on the Pt−GlOH bond energy.

CONCLUSION

The generation of defects on Pt single crystals seems to be an interesting approach to studying the influence of defects on a given reaction. It is a new way of linking models with highly disturbed surfaces and could be used to determine the influence of defects in different chemical and electrochemical reactions.

The electrochemical behavior in acidic media of GlOH oxidation on Pt surfaces exhibits dependence on the surface order. The FTIR spectra elucidate this influence, revealing a potential dependence of the adsorbate coverage and products formed. The highly ordered surface Pt0-100 can oxidize GlOH at lower potentials in comparison to the highly disordered surface Pt100-0.

DFT calculations show that both CO and GlOH bind more strongly to low-coordinated Pt sites in comparison to the bonding when the surface is absent of defects. These results, together with electrochemical and spectroelectrochemical data, suggest that Pt−CO bond breaking may be the GEOR rate-determining step, primarily responsible for the relationship between GEOR onset and defect density.

ASSOCIATED CONTENT

Supporting Information

The Supporting Information is available free of charge on the ACS Publications website at DOI: 10.1021/acscatal.5b00451.

Additional details of the electrochemical results, details of the treament of the FTIR and CV data, and additional details and discussions about DFT calculations (PDF)

AUTHOR INFORMATION

Corresponding Author

*E-mail for P.S.F.: pablo.fernandez@iqm.unicamp.br.

Present Addresses

[#]Chemistry Institute, State University of Campinas, PO Box 6154, 13083-970 Campinas, SP, Brazil.

[∇]Chemical Engineering Department, Federal University of São Carlos, P.O. Box 676, 13565-905 São Carlos, SP, Brazil.

Notes

The authors declare no competing financial interest.

ACKNOWLEDGMENTS

Financial support from the Brazilian agencies is acknowledged: FAPESP (grants 2014/01362-6, 2013/13749-0, 2013/21045-2, and 2013/16930-7), CNPQ (grants 474590/2013-5, 454516/2014-2, 403142/2012-1, 484139/2013-4, 405695/2013-6, and 305494/2012-0), CAPES (grant PNPD20131741-PNPD-USP/SC/QUÍMICA), and FUNDCET (grant 0091/12 and process 23/200.583/2012).

REFERENCES

(1) Pagliaro, M.; Rossi, M. *The Future of Glycerol*, 2nd ed.; Royal Society of Chemistry, Cambridge, 2010' RSC Green Chemistry No. *8*.

(2) Dasari, M.; Kiatsimkul, P.; Sutterlin, W.; Suppes, G. *Appl. Catal., A* **2005**, *281*, 225−231.

(3) Chaminand, J.; Djakovitch, L.; Gallezot, P.; Marion, P.; Pinel, C.; Rosier, C. *Green Chem.* **2004**, *6*, 359−361.

(4) Carrettin, S.; McMorn, P.; Johnston, P.; Griffin, K.; Hutchings, G. *Chem. Commun.* **2002**, *7*, 696−697.

(5) Katryniok, B.; Paul, S.; Belliere-Baca, V.; Rey, P.; Dumeignil, F. *Green Chem.* **2010**, *12*, 2079−2098.

(6) Arechederra, R.; Treu, B.; Minteer, S. *J. Power Sources* **2007**, *173*, 156−161.

(7) Kwon, Y.; Schouten, K.; Koper, M. *ChemCatChem* **2011**, *3*, 1176−1185.

(8) Fernández, P.; Martins, M.; Martins, C.; Camara, G. *Electrochem. Commun.* **2012**, *15*, 14−17.

(9) Coll, D.; Delbecq, F.; Aray, Y.; Sautet, P. *Phys. Chem. Chem. Phys.* **2011**, *13*, 1448−1456.

(10) Liu, B.; Greeley, J. *J. Phys. Chem. C* **2011**, *115*, 19702−19709.

(11) Tereshchuk, P.; Chaves, A. S.; Da Silva, J. L. F. *J. Phys. Chem. C* **2014**, *118*, 15251−15259.

(12) Fernández, P. S.; Martins, C. A.; Angelucci, C. A.; Gomes, J. F.; Camara, G. A.; Martins, M. E.; Tremiliosi-Filho, G. *ChemElectroChem* **2015**, *2*, 263−268.

(13) Gomes, J. F.; Tremiliosi-Filho, G. *Electrocatalysis* **2011**, *2*, 96−105.

(14) Markovic, N. M.; Ross, P. N. *Surf. Sci. Rep.* **2002**, *45*, 121−229.

(15) Lebedeva, N. P.; Koper, M. T. M.; Herrero, E.; Feliu, J. M.; van Santen, R. A. *J. Electroanal. Chem.* **2000**, *487*, 37−44.

(16) Iwasita, T. *Electrochim. Acta* **2002**, *47*, 3663−3674.

(17) Xia, X. H.; Liess, H. D.; Iwasita, T. *J. Electroanal. Chem.* **1997**, *437*, 233−240.

(18) Orts, J. M.; Fernandezvega, A.; Feliu, J. M.; Aldaz, A.; Clavilier, J. *J. Electroanal. Chem. Interfacial Electrochem.* **1990**, *290*, 119−133.

(19) Sun, S. G.; Chen, A. C. *Electrochim. Acta* **1994**, *39*, 969−973.

(20) Markovic, N. M.; Gasteiger, H. A.; Ross, P. N. *J. Phys. Chem.* **1995**, *99*, 3411−3415.

(21) Dima, G. E.; Beltramo, G. L.; Koper, M. T. M. *Electrochim. Acta* **2005**, *50*, 4318−4326.

(22) Souza-Garcia, J.; Ticianelli, E. A.; Climent, V.; Feliu, J. M. *Chem. Sci.* **2012**, *3*, 3063−3070.

(23) Vidal-Iglesias, F. J.; Solla-Gullón, J.; Rodríguez, P.; Herrero, E.; Montiel, V.; Feliu, J. M.; Aldaz, A. *Electrochem. Commun.* **2004**, *6*, 1080−1084.

(24) Tian, N.; Zhou, Z. Y.; Sun, S. G.; Ding, Y.; Wang, Z. L. *Science* **2007**, *316*, 732−735.

(25) Welch, C. M.; Compton, R. G. *Anal. Bioanal. Chem.* **2006**, *384*, 601−619.

(26) Clavilier, J.; Faure, R.; Guinet, G.; Durand, R. *J. Electroanal. Chem. Interfacial Electrochem.* **1980**, *107*, 205−209.

(27) Iwasita, T.; Nart, F. C. In *Advances in Electrochemical Science and Engineering*; Gerischer, H., Tobias, C. W., Ed.; Wiley-VCH: Weinheim, Germany, 1995; Vol. *4*.

(28) Rodríguez, P.; Herrero, E.; Solla-Gullón, J.; Vidal-Iglesias, E. J.; Aldaz, A.; Feliu, J. M. *Electrochim. Acta* **2005**, *50*, 3111−3121.

DOI: 10.1021/acscatal.5b00451
ACS Catal. 2015, 5, 4227−4236

(29) Schnaidt, J.; Heinen, M.; Denot, D.; Jusys, Z.; Behm, R. J. *J. Electroanal. Chem.* **2011**, *661*, 250−264.
(30) Perdew, J. P.; Burke, K.; Ernzerhof, M. *Phys. Rev. Lett.* **1996**, *77*, 3865−3868.
(31) Kresse, G.; Hafner, J. *Phys. Rev. B: Condens. Matter Mater. Phys.* **1993**, *48*, 13115−13118.
(32) Kresse, G.; Furthmuller, J. *Phys. Rev. B: Condens. Matter Mater. Phys.* **1996**, *54*, 11169−11186.
(33) Blochl, P. E. *Phys. Rev. B: Condens. Matter Mater. Phys.* **1994**, *50*, 17953−17979.
(34) Kresse, G.; Joubert, D. *Phys. Rev. B: Condens. Matter Mater. Phys.* **1999**, *59*, 1758−1775.
(35) Vidal-Iglesias, F. J.; Solla-Gullón, J.; Campina, J. M.; Herrero, E.; Aldaz, A.; Feliu, J. M. *Electrochim. Acta* **2009**, *54*, 4459−4466.
(36) Rodríguez, P.; Herrero, E.; Solla-Gullón, J.; Vidal-Iglesias, F. J.; Aldaz, A.; Feliu, J. M. *Electrochim. Acta* **2005**, *50*, 4308−4317.
(37) Solla-Gullón, J.; Vidal-Iglesias, F. J.; Rodríguez, P.; Herrero, E.; Feliu, J. M.; Clavilier, J.; Aldaz, A. *J. Phys. Chem. B* **2004**, *108*, 13573−13575.
(38) Souza-Garcia, J.; Angelucci, C. A.; Climent, V.; Feliu, J. M. *Electrochem. Commun.* **2013**, *34*, 291−294.
(39) Domke, K.; Herrero, E.; Rodes, A.; Feliu, J. M. *J. Electroanal. Chem.* **2003**, *552*, 115−128.
(40) Conway, B. *Prog. Surf. Sci.* **1995**, *49*, 331−452.
(41) Gómez-Marín, A. M.; Clavilier, J.; Feliu, J. M. *J. Electroanal. Chem.* **2013**, *688*, 360−370.
(42) Björling, A.; Feliu, J. M. *J. Electroanal. Chem.* **2011**, *662*, 17−24.
(43) Solla-Gullón, J.; Rodríguez, P.; Herrero, E.; Aldaz, A.; Feliu, J. M. *Phys. Chem. Chem. Phys.* **2008**, *10*, 1359−1373.
(44) Al-Akl, A.; Attard, G.; Price, R.; Timothy, B. *Phys. Chem. Chem. Phys.* **2001**, *3*, 3261−3268.
(45) Koper, M. T. M. *Nanoscale* **2011**, *3*, 2054−2073.
(46) Vidal-Iglesias, F. J.; Arán-Ais, R. M.; Solla-Gullón, J.; Rodríguez, P.; Herrero, E.; Feliu, J. *ACS Catal.* **2012**, *2*, 901−910.

DOI: 10.1021/acscatal.5b00451
ACS Catal. 2015, 5, 4227−4236